SAND--88-3305C

DE90 001093

MULTI-MEGAGAUSS MAGNETIC FIELD GENERATION ON SATURN*

R. B. Spielman, T. W. Hussey, D. L. Hanson, and S. F. Lopez

Sandia National Laboratories, Albuquerque, NM, USA

INTRODUCTION

Very large magnetic fields were first produced using electrical discharges through coils. [1-3] More recently, many researchers have used the method of explosively-driven flux compression to generate megagauss magnetic fields. [4-11] We reported using Proto-II, a 10 TW electrical accelerator, to directly generate fields up to 1.5 kT (15 MG) in a coaxial geometry. [12] The development of even larger electrical accelerators has now allowed us to directly generate magnetic fields of magnitudes equivalent to the largest values attained with explosively-driven flux compression generators. In this paper we report experimental results in which the Saturn accelerator delivered a peak current of 10.5 MA to a 2-mm diameter tungsten rod, thereby generating a peak magnetic field of ~ 2.1 kT (21 MG). We also show the results of one-dimensional (1-D) calculations which show that peak fields of 2.1 kT were achieved at the surface of the tungsten rod. We will discuss possible constraints on the production of megagauss magnetic fields by either direct current generation or by explosively-driven flux compression using metallic liners.

EXPERIMENTAL SETUP

Saturn [13] is a low impedance driver designed for megavolt bremsstrahlung operation (See Fig. 1). Saturn operates at a power of 32 TW, at a voltage of 1.9 MV, with an impedance of 0.111 Ω, and with a 40 ns FWHM voltage pulse. Saturn couples electrical energy from the water pulse-forming lines (PFL)/water transmission lines into the vacuum through a stack of six separate cylindrical insulators. The insulators are 2 m in diameter and are each composed of eight separate, 3.8-cm-high acrylic rings. In the electron beam mode each insulator feeds a biconic disk magnetically-insulated transmission line (MITL), each pair of which produces an annular electron beam. For z-pinch or high current experiments we configure the machine with four biconic MITLs feeding a single disk MITL through a double

*This work was performed under the auspices of the U.S. Department of Energy by Sandia National Laboratories under Contract DE-AC04-76DP00789.

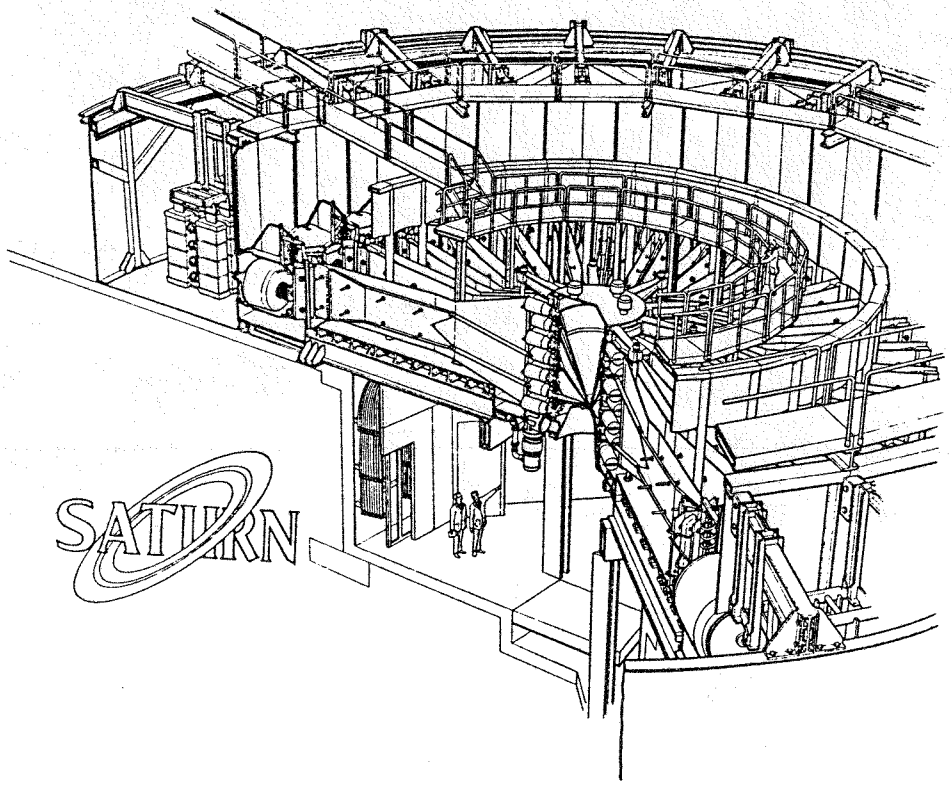

Figure 1. An artists drawing of Saturn.

post-hole vacuum convolute. Available machine energy is not reduced because the electrical energy in the water transmission lines is rerouted only through the four insulator stacks that are used.

The Saturn double post-hole convolute [14] uses an anode post/cathode hole configuration to couple the conical transmission lines together. There are two sets of six posts and holes (one set for each anode pair and cathode) hence the origin of the name "double post-hole convolute". We used six posts, 1 cm in diameter, located 7.6 cm from the axis of cylindrical symmetry to connect the anodes together. The cathode holes are slightly elliptical in shape with a 1-cm minimum gap to the posts (radially inward from the posts). The cathodes are connected together with a cylindrical skirt inside the diameter of the convolute posts. A schematic of the double post-hole convolute is shown in Fig. 2.

The load consisted of a coaxial inductor with an inner diameter of 0.2 cm and an outer diameter of 0.7 cm. All of the mechanical hardware inside a 2-cm radius was fabricated from Kenertium, a tungsten alloy. The total length of the coaxial inductor was 1 cm. The load inductance was 2.5 nH. Including the inductance of the remainder of the electrical feed, the total inductance of the electrical circuit was ~ 10 nH. The dimensions of the coaxial load on Saturn were the same as those of the earlier Proto-II experiments. [12] (See Figs. 3-4.)

The inner conductor diameter was chosen to maximize the magnetic field. Instability-driven deformation of the inner conductor would be a problem if the inner conductor were too small in diameter or if the material density were too low. Too large an inner conductor would have reduced the peak magnetic field. Our preliminary calculations indicated that a 2-mm diameter tungsten conductor would satisfy our concerns for these experiments.

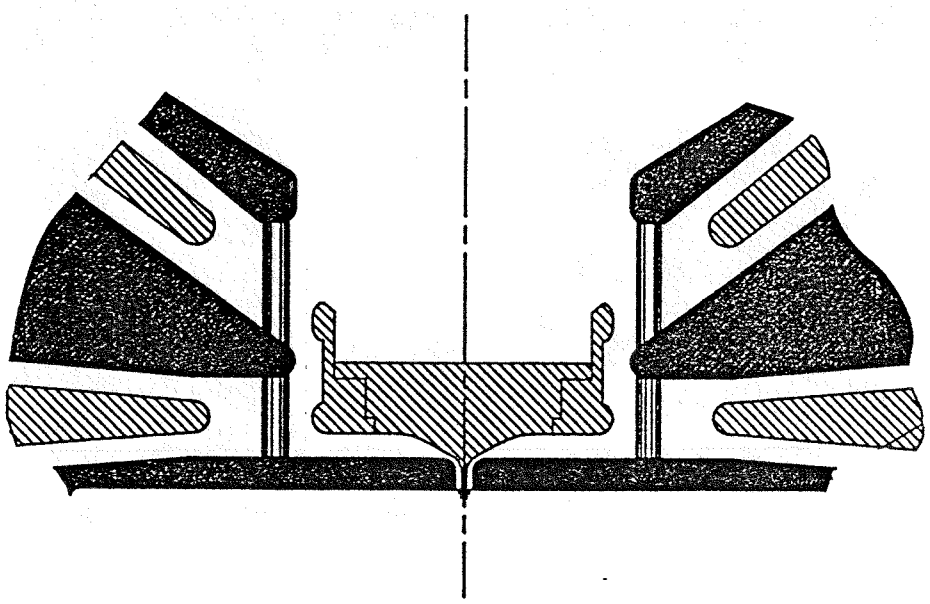

Figure 2. A schematic of the Saturn double post-hole vacuum convolute and load showing the anodes (solid) and cathodes (shaded).

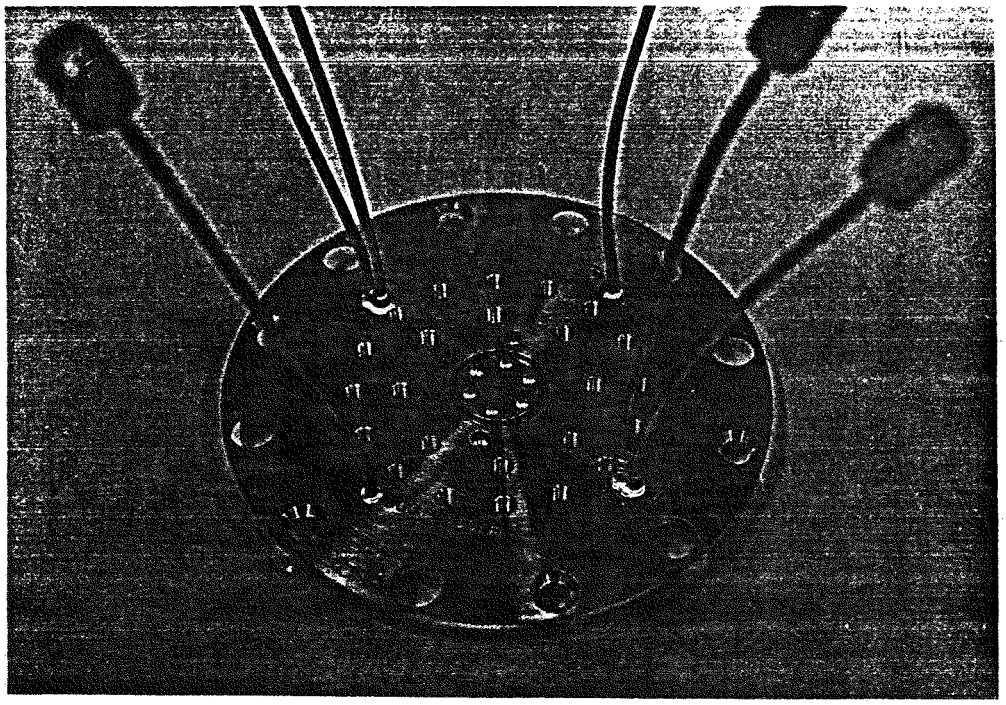

Figure 3. A picture of the lower anode and the tungsten load showing the B-dot current monitors.

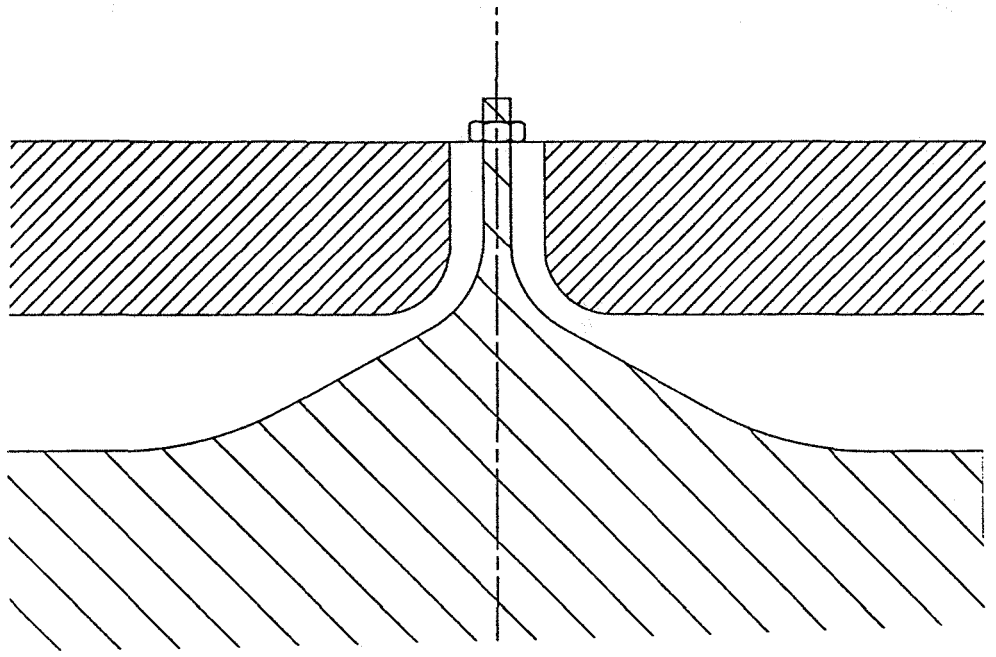

Figure 4. A schematic of the load as installed in Saturn.

Current monitors included segmented, self-integrating Rogowski coils located at the insulator stack on each level to measure the current external to the plastic/vacuum interface, two stainless-steel resistive current shunts placed in each of the conical MITLs to measure the current in the vacuum transmission line, and calibrated B-dot loops and lithium-niobate pressure transducers to measure the total current near the load. [15] The radiation environment near the load made a direct measurement of the peak magnetic field very difficult. Future experiments may use Zeeman splitting of well known emission lines as a magnetic field diagnostic.

DATA

The experimental data consisted of the electrical signals from the segmented Rogowski coils, resistive current shunts, B-dot loops, (on two shots) lithium-niobate stress gauge data, and observations of the physical hardware. Measurement of current, together with the known inductance of the load, gave a good check on energy balance. The current traces from the highest current shot are shown in Fig. 5. The current, measured by the load B-dot, rises to a peak value of 10.5$\pm$.5 MA in about 50 ns. Assuming that all of the current is flowing inside a radius of 1 mm, the generated magnetic field at a 1-mm radius was ~ 2.1 kT (21 MG). The measured inductance of the load was 10$\pm$1 nH (10.3 nH calculated inductance). From the measured current we inferred a peak stored magnetic energy of 600$\pm$60 kJ. A comparison of the accuracy of the B-dot probes was made with the lithium-niobate stress gauges. Fig. 6 shows the comparison of the B-dot data and the lithium-niobate stress gauge data from a lower current shot. The data agree to within 3%. The B-dot probes fail at 160 ns due to electrical flashover and the recording time of the lithium-niobate gauge is limited to ~ 80 ns because of the shock transit time of the lithium-niobate.

There was no visible damage to the MITL hardware, indicating no electrical losses and full current delivery to the load. The load, consisting of the 0.2-cm diameter center conductor and the adjacent return current walls, was completely vaporized. (See Fig. 7) This damage

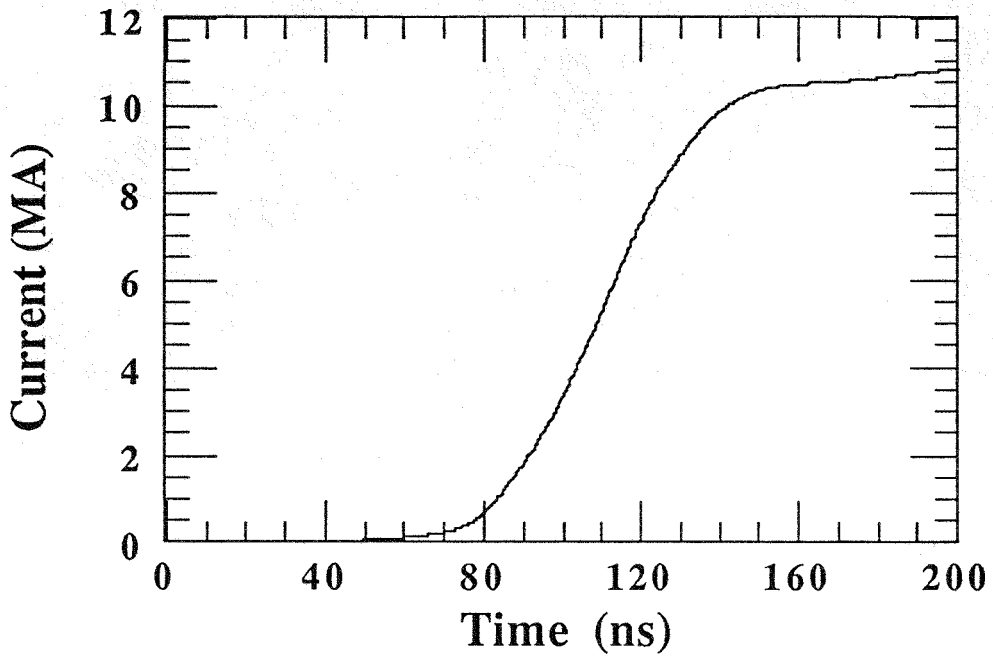

Figure 5. Saturn current waveform from a B-dot probe. The monitor failed at 160 ns.

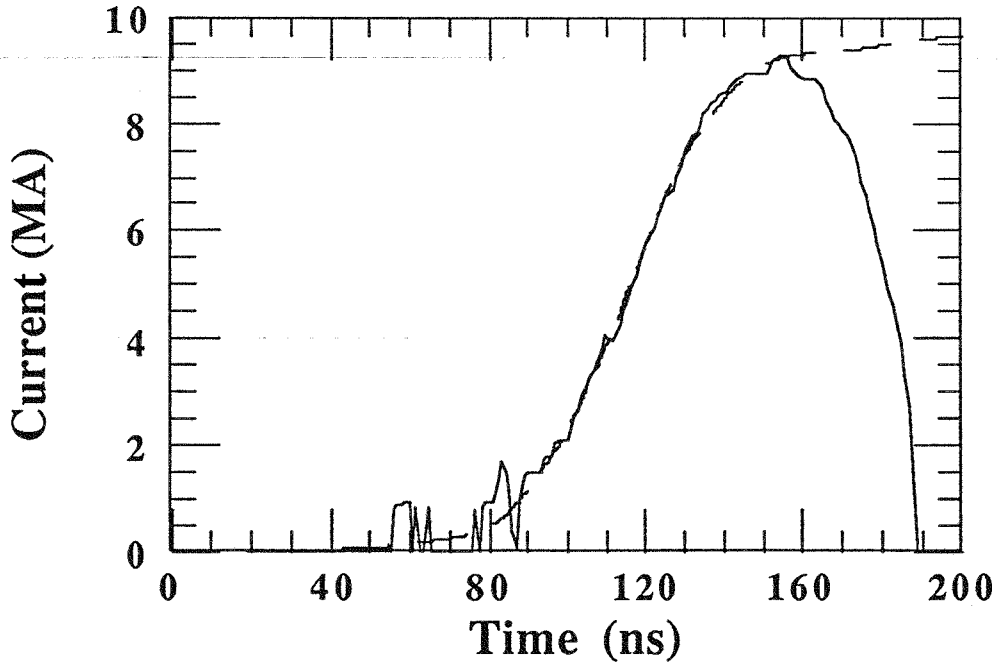

Figure 6. A comparison of current data from a lithium-niobate pressure transducer (solid line) and calibrated B-dot probes (dashed line).

was consistent with the expected ohmic and shock heating of the hardware. The peak less steel transmission line hardware inside a 10-cm radius was severely deformed by the large magnetic pressures. On another shot where the current was measured with lithium-niobate stress gauges to be 9 MA at 2.2-cm radius, physical damage to the small radius hardware was less severe.

CALCULATIONS

One-dimensional MHD calculations, including radiation-loss effects, have been performed in which the Saturn driver was modeled by a time-dependent open-circuit voltage waveform. Three cases were modeled, each assuming a 10-nH inductance, a 0.111-Ω impedance, a 1.25-cm gap spacing, and a 7-mm radius return conductor, with the following inner conductors:

1. 2-mm diameter tungsten rod
2. 1-mm diameter tungsten rod
3. 2-mm diameter aluminum rod.

The first case corresponds to the experiment described here, while cases 2 and 3 are shown for comparison and to motivate the choice of experimental parameters.

Figure 8 shows magnetic field at the inner conductor surface as a function of time for the three cases. Note that t = 0 in the calculations does not correspond to that assumed for the

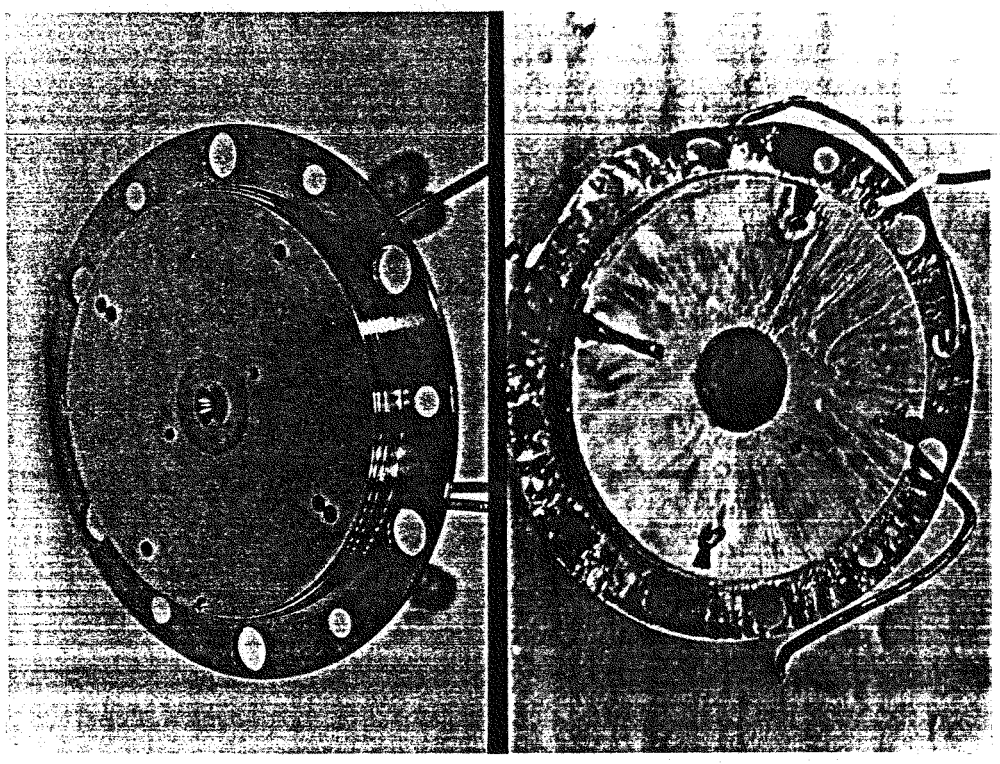

Figure 7. A picture of the tungsten anode before (left) and after (right) a shot.

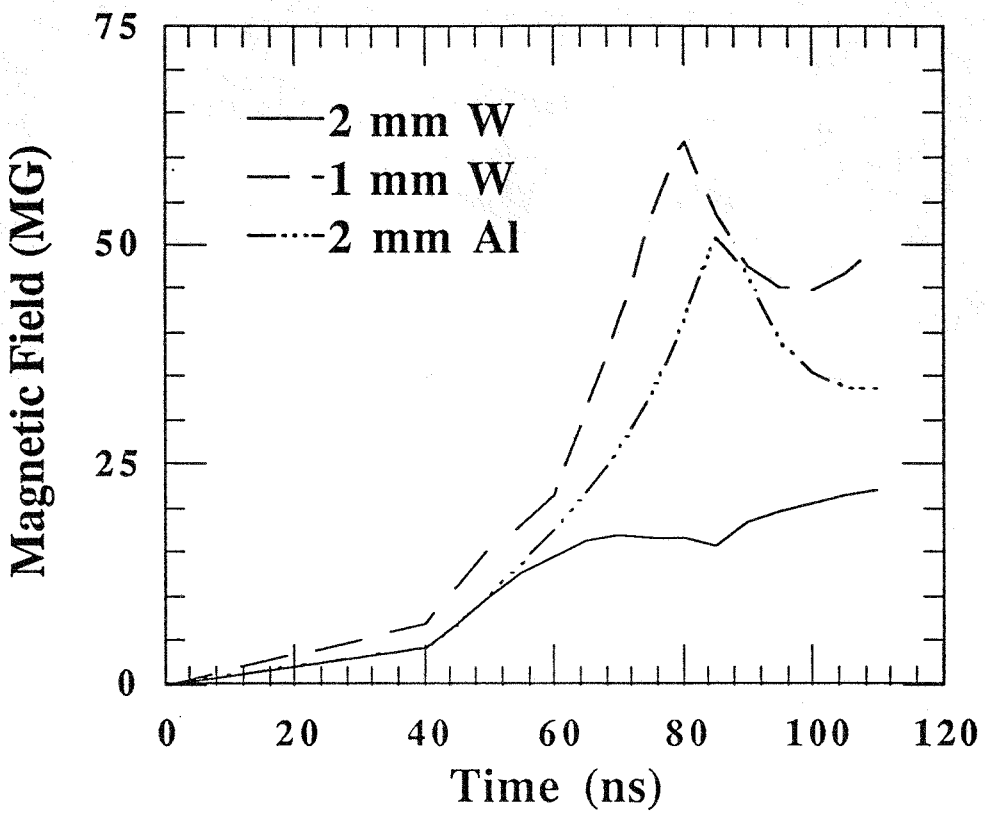

Figure 8. Magnetic field (at the outer boundary of the center conductor) as a function of time from the 1-D MHD calculations for the three cases.

experimental data. Note also that the peak field in cases 2 and 3 greatly exceeds that of case 1. These peak magnetic fields (in MG) are also found to exceed,

$$B = \frac{.2\ I_{max}}{r_0}, \qquad (1)$$

in cases 2 and 3, where I_{max} = 11.5 MA is the approximate peak current (in MA) and r_0 is the initial radius (in cm). This is due to compression of the rod by magnetic forces, shown as a function of time for the three cases in Fig. 9. The calculated current profiles, shown in Fig. 10, are quite similar for the three cases, though the effect of the higher inductance of the 1-mm tungsten rod is illustrated by the slower rise of the current at early time for that case.

In order for very high fields to be present in this system, the current channel must remain quite small (i.e. of the order of the initial radius). Since the post is a relatively good conductor (mean electron temperature = 10's of eV at peak current), we expect this current channel to be well defined unless it is disrupted by a magneto-hydrodynamic m = 0 instability. It is important to remember that the 1-D calculations described above fail to include the effects of 2- or 3-D instabilities. The growth rate for this process can be roughly approximated (for the most damaging mode) by the inverse Alfven transit time;

$$\gamma_a \sim \frac{V_a}{r_0}, \tag{2}$$

where the Alfven velocity is given by;

$$V_a = \frac{B}{\sqrt{4\pi\rho}}, \tag{3}$$

ρ is the conductor mass density, and r_0 is the initial radius of the inner conductor (CGS units). For case 1 (2-mm diameter tungsten) this gives $\gamma_a \sim 1.28X10^7$ s^{-1}, for case 2 γ_a is $5.12X10^7$ s^{-1}, while for case 3 it is $3.43X10^7$ s^{-1}. Since this estimated Alfven growth rate varies inversely with radius, and since its effect on the pinch depends on its duration, we show it as a function of time in Fig. 11 with $r_0 \rightarrow r(t)$, $B_{max} \rightarrow B(t)$, and $\rho_0 \rightarrow \rho(t)$. We note that, because of compression, γ_a exceeds $5.0X10^7$ (20 ns growth time) well before peak current in cases 2 and 3, whereas in case 1 a growth rate of $1.28X10^7$ s^{-1} (80-ns growth time) is not exceeded until current maximum is obtained. This suggests that case 1 is a conservative configuration, and the center conductor should maintain its integrity until well past peak current, whereas in cases 2 and 3, though they apparently obtain somewhat higher fields, the center conductors can be expected to disrupt hydrodynamically during the pulse.

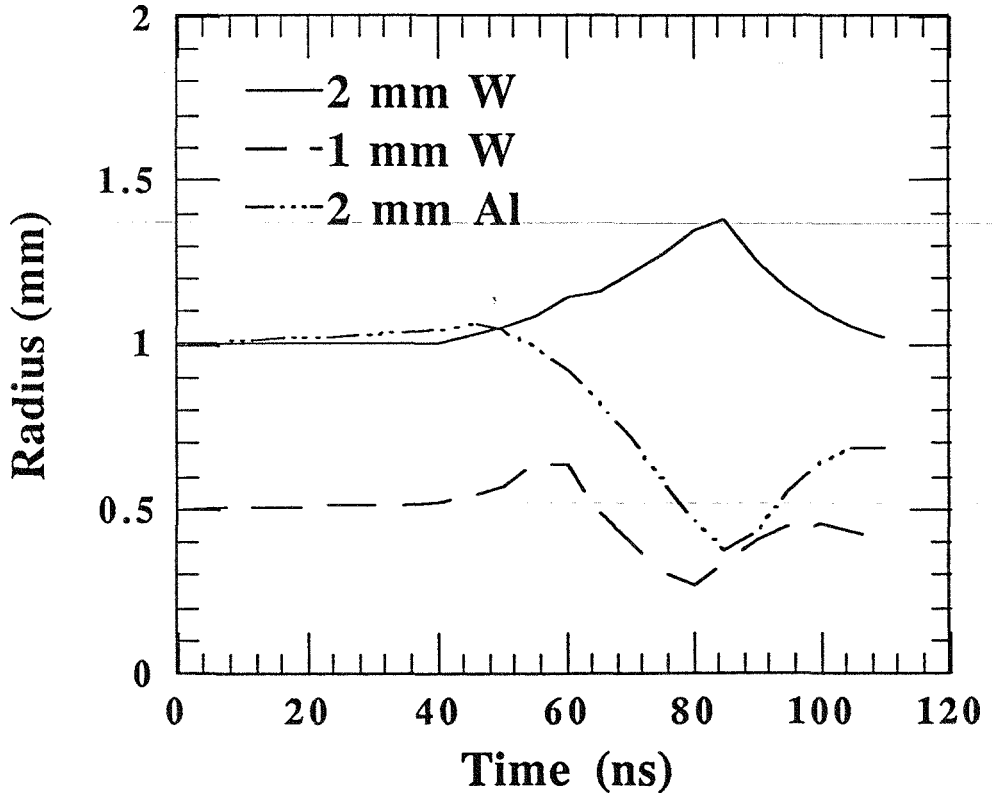

Figure 9. The position of the boundary of the center conductor from 1-D MHD calculations as a function of time for the three cases.

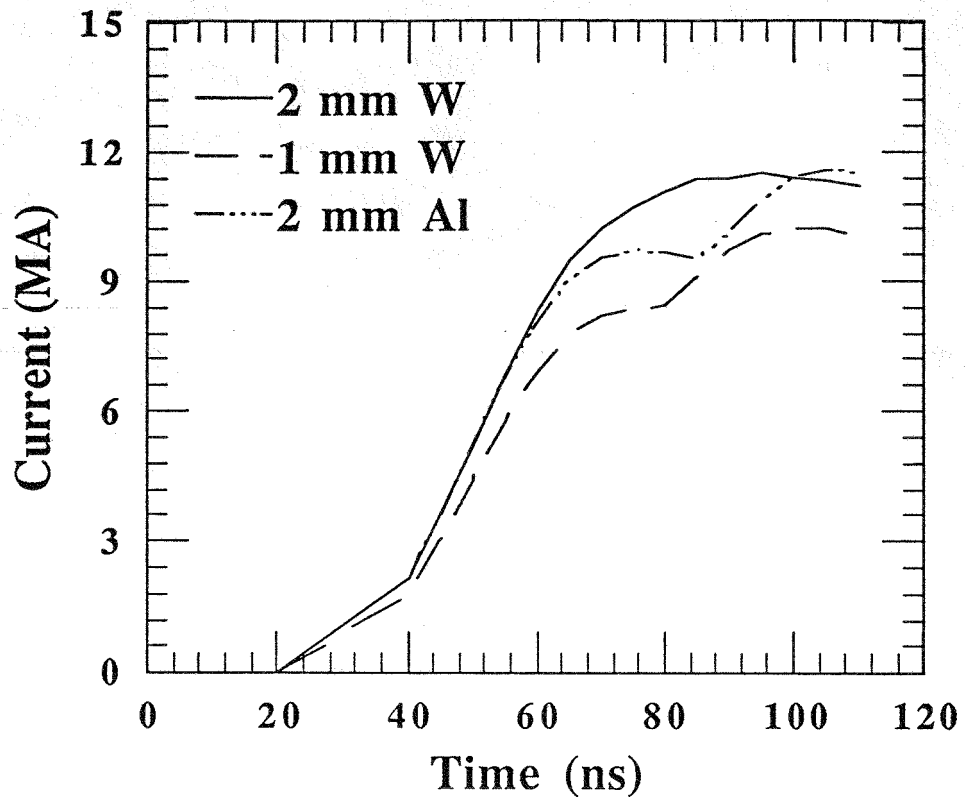

Figure 10. The calculated current profiles for the three cases.

LIMITS ON THE MAXIMUM ATTAINABLE MAGNETIC FIELD

One can now examine the constraints placed on conductor size by the current applied to the system. The pulse length of the driver together with the mass density of the conductor yield an expression for the peak magnetic field as a function of current. Using equations 1-3 we find that the peak magnetic field scales as;

$$B \propto \left[\frac{I\sqrt{4\pi\rho}}{\tau}\right]^{.5}. \qquad (4)$$

Where τ is the rise time of the current pulse. We see that in order to satisfy the rough stability constraints indicated by the Alfven time, the maximum attainable magnetic field scales as $I^{.5}$ rather than as I. This observation combined with the increasing level of losses (not discussed in this paper) from Ohmic, shock, and compressional heating of the center conductor which are increasing as I^2 or faster [16] imply that there is likely a constraint on the size of magnetic fields that can be produced by direct current generation.

This fact also has implications for magnetic flux compression using metallic liners. The compressed magnetic fields are sustained by the very large induced eddy currents in the liner

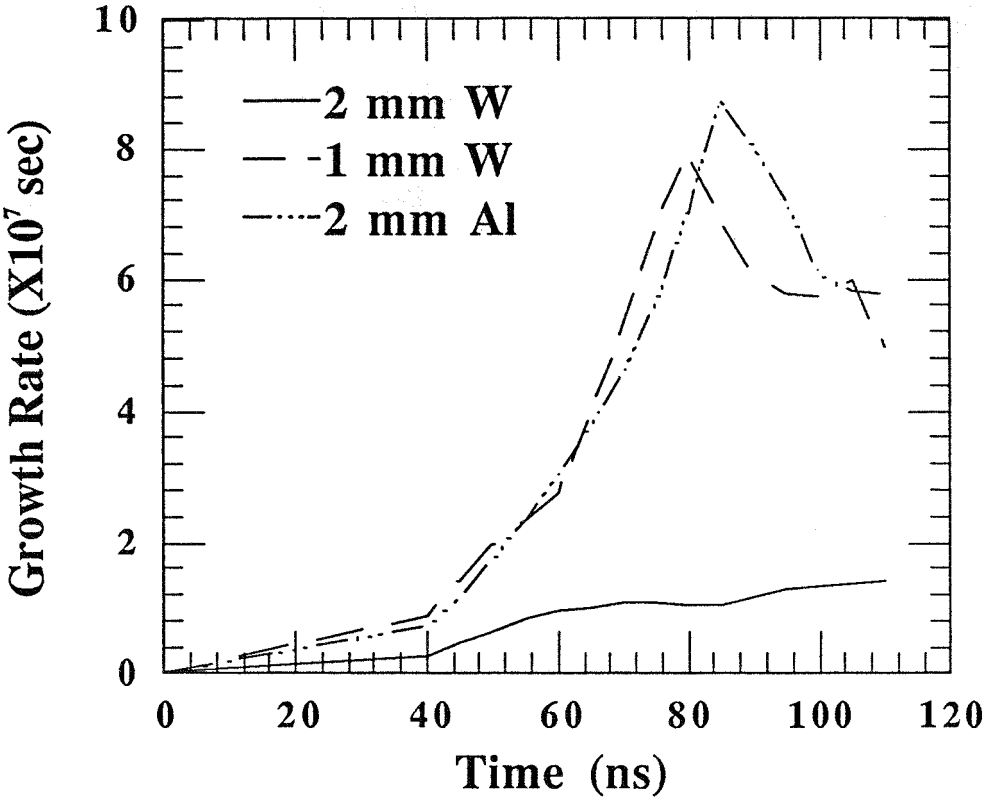

Figure 11. The instability growth rates as a function of time for the three cases.

walls. These current densities must approach the same levels seen in direct current production for equivalent magnetic fields. While the instabilities driven by azimuthal currents (or axial magnetic fields) differ slightly from axial currents, the same general limitations on the maximum value of magnetic fields apply.

CONCLUSIONS

We have passed 10.5 MA through a 2-mm diameter tungsten conductor generating approximately 2.1-kT (21-MG) magnetic fields. Computer modelling of the interaction of the magnetic field and the inner conductor indicates that the conductor is slowly compressed for the duration of the current pulse. While we believe that dissipative processes, such as resistive and shock heating, in the conductors constitute a significant energy loss for the system, these losses to not represent a limit on current density or magnetic field. If magnetic fields are generated either directly by applied currents in solid conductors or indirectly by metallic-liner driven, magnetic-flux compression techniques, then hydrodynamic instabilities, driven by the local magnetic field, constitute a limit on current density and magnetic field. The maximum attainable magnetic field scales as $I^{.5}$.

ACKNOWLEDGEMENTS

We gratefully acknowledge the enthusiastic support of the Saturn operations crew.

REFERENCES

[1] P. Kapitza, Proc. R. Soc. A 105, 691 (1924).
[2] S. Foner and H. H. Kolm, Rev. Sci. Instr. 27, 547 (1956).
[3] H. P. Furth, M. A. Levine, R. W. Waniek, Rev. Sci. Instr. 28, 949 (1957).
[4] Ya. P. Terletskii, Zh. Eksp. Teor. Fiz. 32, 381, (1957).
[5] C. M. Fowler, W. B. Garn, and R. S. Caird, J. Appl. Phys. 31, 558 (1960).
[6] F. Herlach, and H. Knoepfel, Rev. Sci. Instr. 36, 1088 (1965).
[7] H. Knoepfel and F. Herlach, eds., Proc. Conf. on Megagauss Magnetic Field Generation by Explosives and Related Experiments, Frascati, Sept. 21-23, 1965, Euratom EUR2750.e, Bruxelles (1966).
[8] A. D. Sakharov, R. Z. Lyudaev, E. N. Smirnov, Yu. I. Plyushchev, A. I. Pavloskii, V. K. Chernyshev, E. A. Feoktistova, E. I. Zharinov, and Yu. I. Zysin, Dokl. Akad. Nauk. SSSR 165, 65 (1965).
[9] E. C. Cnare, J. Appl. Phys. 37, 3812 (1968).
[10] P. J. Turchi, ed., Megagauss Physics and Technology, Plenum Press, New York (1980).
[11] V. M. Titov, and G. A. Shvetsov, eds., Ultrahigh Magnetic Fields, Nauka, Moscow (1984).
[12] R. B. Spielman, T. W. Hussey, and S. F. Lopez, Megagauss Technology and Pulsed Power Applications, edited by C. M. Fowler, R. S. Caird, and D. J. Erickson (Plenum Press, New York, 1987), p. 167.
[13] D. D. Bloomquist, R. W. Stinnett, D. H. McDaniel, J. R. Lee, A. W. Sharpe, J. A. Halbleib, L. G. Schlitt, P. W. Spence, and P. Corcoran, Proc. of the Sixth IEEE Pulsed Power Conference, Arlington, VA edited by P. J. Turchi and B. H. Bernstein (IEEE, New York, 1987), p. 310.
[14] R. B. Spielman, P. Corcoran, J. Fockler, H. Kishi, P. W. Spence, Proc. of the Seventh IEEE Pulsed Power Conference, Monterey, CA (1989).
[15] D. L. Hanson, R. R. Williams, J. L. Porter, R. B. Spielman, M. K. Matzen, to be published.
[16] S. Singer and R. O. Hunter, Proc. of the 3rd IEEE Int. Pulsed Power Conf., Albuquerque, NM, p. 351 (1981).